Available online at www.sciencedirect.com
ScienceDirect
Powder Technology 170 (2006) 53 – 63
POWDER TECHNOLOGY
www.elsevier.com/locate/powtec

Determination of coalescence kernels for high-shear granulation using DEM simulations

Justin A. Gantt [a], Ian T. Cameron [b], James D. Litster [b], Edward P. Gatzke [a,*]

[a] Department of Chemical Engineering, University of South Carolina, Columbia, SC 29208, USA
[b] Particle and System Design Centre, Division of Chemical Engineering, University of Queensland, St. Lucia, QLD AU 4072

Received 4 October 2005; received in revised form 2 August 2006; accepted 4 August 2006
Available online 15 August 2006

Abstract

Discrete element method (DEM) modeling is used in parallel with a model for coalescence of deformable surface wet granules. This produces a method capable of predicting both collision rates and coalescence efficiencies for use in derivation of an overall coalescence kernel. These coalescence kernels can then be used in computationally efficient meso-scale models such as population balance equation (PBE) models. A soft-sphere DEM model using periodic boundary conditions and a unique boxing scheme was utilized to simulate particle flow inside a high-shear mixer. Analysis of the simulation results provided collision frequency, aggregation frequency, kinetic energy, coalescence efficiency and compaction rates for the granulation process. This information can be used to bridge the gap in multi-scale modeling of granulation processes between the micro-scale DEM/coalescence modeling approach and a meso-scale PBE modeling approach.

Keywords: Granulation; Discrete element method; Coalescence

1. Introduction

Granulation is a size enlargement technique where growth of small, dry particles is promoted through liquid binder addition and process agitation. Modeling of granulation processes has progressed significantly in recent years due to an improved understanding of powder mechanics [1]. Fundamental knowledge of physical granular interactions can be analyzed on several scales. The bulk of granulation research has occurred at the meso- and macro-scales [2]. Due to increased interest in design of particles, focus has shifted to a better understanding of the micro-scale. Modeling methods such as discrete element method (DEM) are beginning to bridge the gap between micro- and meso-scales [2].

Meso-scale modeling can best be described as modeling based on analysis of the rate processes that control physical particle property dynamics. This modeling is typically performed using population balance equations (PBEs). PBEs provide an efficient and accurate way to model the complicated factors associated with rates of particle wetting, nucleation, consolidation, growth and breakage. PBEs determine rates of coalescence based on coalescence kernels. Some of the original coalescence kernels proposed in the 1960s are based on purely empirical model techniques [3–7]. As the understanding of the physics behind particulate interactions improve, coalescence kernels have become more realistic. Adetayo and Ennis created a kernel based on a critical granule cut-off size at which coalescence becomes impossible [8]. This cut-off size was based on Stokes regime analysis. Liu and Litster proposed a physically based kernel derived from a hertzian model for deformable surface wet granules [9]. This model will be used for coalescence efficiency analysis in the current work.

Micro-scale particle analysis is performed by two techniques simultaneously. A complex coalescence model is used to determine the agglomeration efficiency of individual particle interactions, while a DEM simulation is used to predict particle collisions at the micro-scale. A comprehensive understanding of inter-particle forces, viscous effects and mechanical effects of particle interactions will greatly enhance the ability to model agglomeration efficiency. Micro-scale analysis of particle flow patterns can be performed using DEM modeling techniques.

* Corresponding author. Tel.: +1 803 777 1159.
E-mail address: gatzke@sc.edu (E.P. Gatzke).

0032-5910/$ - see front matter © 2006 Elsevier B.V. All rights reserved.
doi:10.1016/j.powtec.2006.08.002

The DEM uses simple mechanical models to calculate contact forces. In this paper, the contact forces were modeled based on Cundall and Strack's soft sphere DEM [10]. This type of model expresses forces with the use of a spring, dash-pot and slider. The length and time scales at the micro-scale differ significantly from meso-scale problems; therefore, novel schemes which couple the two scales become an important issue. This paper presents a technique to integrate the multi-scale behavior by determining coalescence kernels and compaction rate constants from a DEM algorithm which utilizes a realistic model of deformable surface wet granules.

2. Soft-sphere DEM

Discrete element method techniques are an ideal way to model particle interactions. The goal of this work is to examine the multi-scale nature of the process, not to model every specific particle and particle interaction in a granulator. Therefore, there will be several assumptions used to simplify the high-shear granulation process:

1. *A soft-sphere DEM model is applicable*: hard sphere contact models may result in inelastic collapse, rendering the model ineffective and impractical for multi-scale modeling. Furthermore, soft-sphere models have been proven to model granular flow for dense particle flows such as found in a high-shear mixer. A soft-sphere model as proposed by Cundall and Strack [10] will be used.
2. *A flat-plate rotor is used*: high-shear mixers are classified by their use of moving parts to create bed agitation. A moving impeller blade creates significant modeling complexity. Therefore, a flat plate rotor is used to create the agitation. Such a simplification was successfully applied by Muguruma et al. [11].
3. *Periodic boundaries are applied to reduce particle number*: periodic boundaries reduce the total number of particles necessary for simulating a control volume. Cartesian periodic boundaries have been applied for molecular dynamics applications, but to maintain the proper motion in the mixer, cylindrical boundaries must be applied. A π/32 wedge control volume is used in this work.
4. *Only particle motion is accounted for in the DEM simulation*: no coalescence, compaction or breakage takes place in the DEM simulation. A coalescence model is used to predict growth based on data gathered from a DEM simulation. This allows the DEM simulation to track particle motion where the particle size distribution and number of particles is constant.
5. *Drag forces are negligible*: The only forces which will be accounted for are particle–particle collision forces, particle–wall collision forces and gravitation forces. Viscous forces are indirectly accounted for because the coalescence model which accounts for viscous interactions is used to predict the coefficient of restitution.
6. *The DEM and coalescence models are complementary*: neither model by itself is an adequate means of calculating a coalescence kernel. The two models work separately in parallel. The DEM model is dynamic and is capable of predicting collision rates and contact forces. The coalescence model depends on not only forces, but mechanical properties of the particles as well.

2.1. Particle motion

The DEM technique allows for a greater understanding of the overall behavior of particles by tracking each particle individually. It is now possible to analyze the behavior of a large collection of free flowing particles by observing the trajectories of each particle separately. Each individual particle trajectory can be solved by integrating Newton's equations of motion. The equation of translational particle motion and rotational motion is given by:

$$m\frac{\mathrm{d}\vec{\mathrm{v}}}{\mathrm{d}t} = m\vec{\mathrm{g}} + \vec{\mathrm{F}}_{\mathrm{c}} + \vec{\mathrm{F}}_{\mathrm{w}} \tag{1}$$

$$I\frac{\mathrm{d}\vec{\mathrm{w}}}{\mathrm{d}t} = \vec{\mathrm{M}}_{\mathrm{c}} + \vec{M}_{\mathrm{w}} \tag{2}$$

where m is the mass of the particle, $\vec{\mathrm{v}}$ is the particle velocity vector, $\vec{\mathrm{g}}$ is the gravitational acceleration vector, $\vec{\mathrm{F}}_{\mathrm{c}}$ is the sum of the forces on the particle caused by other particles, $\vec{F}_{\mathrm{w}}$ is the sum of the forces on the particle caused by the walls of the equipment, I is the inertia, $\vec{\mathrm{w}}$ is the particle rotation velocity vector, and $\vec{\mathrm{M}}$ is the moment vector resulting from particle–particle or particle–wall collisions.

The future velocities and positions following the current time step can be calculated by applying a forward Euler approximation to Eq. (1). This can be calculated explicitly as:

$$\vec{r} = \vec{r}_0 + \vec{v}_0\Delta t \tag{3}$$

$$\vec{v} = \vec{v}_0 + \left(\frac{\vec{F}_{\mathrm{c}}}{m} + \frac{\vec{F}_{\mathrm{w}}}{m} + \vec{g}\right)\Delta t \tag{4}$$

$$\vec{w} = \vec{w}_0 + \left(\frac{\vec{M}_{\mathrm{c}}}{I} + \frac{\vec{M}_{\mathrm{w}}}{I}\right)\Delta t \tag{5}$$

Here $\vec{\mathrm{r}}$ is the position vector of the particle at the following time step, $\vec{r}_0$ is the position vector at the current time step, $\vec{v}_0$ is the velocity vector at the current time step, $\vec{w}_0$ is the rotational velocity vector at the current time step, Δt is the length of the time step, and $\vec{\mathrm{v}}$ is the velocity vector at the following time step. Note that this problem is formulated in the x, y and z directions.

2.2. Contact forces

Contact forces resulting from particle/particle and particle/wall collisions are be modeled using a spring, dash-pot and slider as first described by Cundall and Strack [10]. This technique separates forces into normal and tangential forces as shown in Fig. 1.

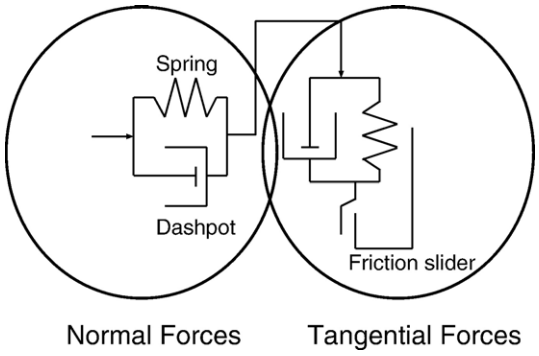

Fig. 1. Model of normal and tangential contact forces. Adapted from Tsuji et al. [27].

The normal collision velocity, $\vec{v}_n$, is given by:

$$\vec{v}_n = (\vec{v}_r \cdot \vec{n})\vec{n} \tag{6}$$

where the normal unit vector, $\vec{n} = (r_2 - r_1)/|r_2 - r_1|$ and the relative velocity is defined as $\vec{v}_r = \vec{v}_1 - \vec{v}_2$. Furthermore, the tangential collision velocity, $\vec{v}_t$, is defined as:

$$\vec{v}_t = \vec{v}_r - \vec{v}_n \tag{7}$$

where the tangential unit vector is defined as $\vec{t} = \frac{\vec{v}_t}{|\vec{v}_t|}$. A simple linear spring and dash-pot model is used for the normal contact force. The tangential contact force is derived from a viscous shear force model, which takes into account tangential elasticity. The normal, $\vec{F}_n$, and tangential contact force, $\vec{F}_t$, are then defined as:

$$\vec{F}_n = -k\vec{\xi}_n - \eta(\vec{v}_r \cdot \vec{n})\vec{n} \tag{8}$$

$$\vec{F}_t = -\min(-k\xi, |\mu \vec{F}_n|) \cdot sign(\zeta) \tag{9}$$

where k is the spring constant, η is the damping coefficient, μ is the coefficient of friction and ξ is the tangential overlap:

$$\xi(t) = \int_{t_0}^{t} v_t(t')dt' \tag{10}$$

In the situation where simultaneous collisions occur between particles in densely packed particle flows, these forces are summed to determine a total force. Contact forces for particles and walls are calculated only using different values for stiffness, damping and coefficient of friction. Each of these parameters must be specified based on the physical properties of the granules and the walls.

A large number of time steps are required to capture the dynamics of each collision. An insufficient number of time steps tends to produces an unnatural response. A spring constant is chosen so that the duration of the collision, t_d, lasts approximately 100 time steps, $\Delta t = t_d/100$. The spring constant can then be defined as a function of the contact duration [12]:

$$k = \frac{(\eta t_d)^2 + (2\pi m_e)^2}{4 m_e t_d} \tag{11}$$

where $m_e = \frac{m_1 m_2}{m_1 + m_2}$ and η is the particle damping. This tends to produce spring constants which are smaller than those reported experimentally, but it allows for stable calculations which do not result in unnecessarily long computation times. The damping term, η, can also be defined as a function of the contact duration [12]:

$$\eta = -\frac{2m_{eff}}{t_d}\ln e \tag{12}$$

where e is the coefficient of normal restitution. This value is dependent on extenuating properties such as the collision velocity and extent of deformation. This will be considered in additional detail in Section 3.

3. Coalescence model

To determine if granules coalesce during the DEM simulation, a model for deformable wet granules derived by Liu et al. [13] is used. The model accounts for the mechanical properties of the particles in motion as well as the viscous effects of a liquid layer at the surface. The model shows that dissipation of kinetic energy is first caused by the viscous forces of the binder layer. If the kinetic energy is not completely dissipated by the binder layer, then collision energy and elastic energy of the granules also contribute to dissipation. If all the energy is not dissipated, then the particles rebound. The coefficient of restitution is then calculated based on the dissipated energy.

Liu and Litster define two modes of coalescence based on the collision kinetic energy. Type I coalescence results from collisions where the kinetic energy is completely dissipated by the viscous forces of the binder layer. This results in coalescence before the surface collision through the liquid bridge. Type II coalescence occurs when particles collide and deform, resulting in elastic energy, which cause a retraction of the particles. If the released elastic energy is dissipated by the binder layer, then type II coalescence occurs, if not, rebound occurs. See Fig. 2 for a diagram of this phenomenon. As two particles come into contact with one another, their relative velocities and normal contact forces are calculated using the DEM simulation. These forces, along with the porosity and moisture content of the granule, determine whether a particle will coalesce or rebound.

As binder layers touch during a collision, viscous forces contribute to the slowing of granules. If the collision velocity through the binder layer is less than zero, then type I coalescence occurs before granule surfaces touch. This condition, defined by [13], is shown in Eq. (13).

Type I coalescence:

$$St_v < \ln\left(\frac{h_0}{h_a}\right) \tag{13}$$

where h_0 is the thickness of the binder layer, h_a is the height of the surface asperities and St_v is the viscous Stokes number, a ratio of viscous forces to kinetic forces.

If particles remain in motion, the elastic energy of the collision can be calculated to see if this energy is capable of being

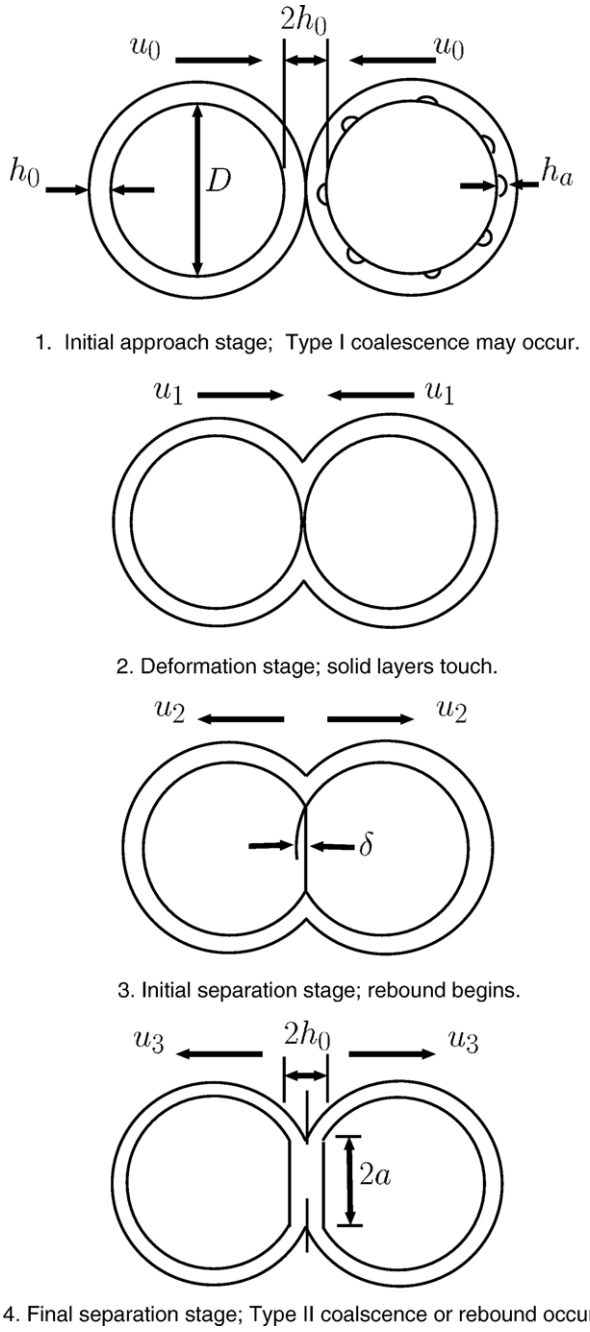

Fig. 2. Model used for coalescence criteria. Adapted from Liu et al. [13].

dissipated by the binder layer. If so, type II coalescence occurs, if not, rebound occurs. The condition for type II coalescence is derived in [13] and displayed in Eq. (14):

Type II coalescence:

$$\sqrt{\frac{Y_d}{E^*}}St_{def}^{(-9/8)} < \frac{0.172}{St_v}\left(\frac{\tilde{D}}{h_0}\right)^2\left[1-\frac{1}{St_v}\ln\frac{h_0}{h_a}\right]^{5/4} \times\left[\left(\frac{h_0^2}{h_a^2}-1\right)+\frac{2h_0}{\delta''}\left(\frac{h_0}{h_a}-1\right)+\frac{2h_0^2}{(\delta'')^2}\ln\left(\frac{h_0}{h_a}\right)\right] \times\left\{1-7.36\frac{Y_d}{E^*}St_{def}^{-1/4}\left[1-\frac{1}{St_v}\ln\frac{h_0}{h_a}\right]^{-1/2}\right\}^2 \quad (14)$$

Here Y_d is the granule yield strength, $E*$ is the granule Young's modulus, St_{def} is the Stokes deformation number, and δ'' is the permanent particle deformation. At each time step in the DEM simulation, as particle–particle contacts are detected, each of these parameters must be updated as new relative collision velocities are calculated. As particles rebound, the coefficient of restitution varies with impact velocity according to the following expression, also derived by Liu et al. [13]:

$$e = 2.46\sqrt{\frac{Y_d}{E^*}}St_{def}^{-1/8}\left[1-\frac{1}{St_v}\ln\frac{h_0}{h_a}\right]^{-1/4} \quad (15)$$

The coefficient of restitution is then used to calculate the damping and spring constant from Eq. (12).

4. DEM simulation conditions

Simulation conditions are listed in Table 1. All particles are assumed to be spherical. It is assumed that the binder in excess of the critical internal saturation is uniformly distributed in a layer of thickness, h_0. Two simulations are analyzed: one with a high viscosity and one with a low viscosity binder. The solid used for the simulation was calcium carbonate, $CaCO_3$. The high viscosity binder is silicon oil and the low viscosity binder is water.

Periodic boundaries were applied to this simulation for a π/32 section of the mixer. This reduces the total number of particles in the simulation by 1/64. 5000 particles are used in the simulation to occupy the π/32 region of interest. Application of

Table 1
Initial conditions for simulation

Parameter	Value
Equipment parameters	
Mixer radius, D_m	0.212 [m]
Mixer height, H_m	0.15 [m]
Impeller speed, w	1000 rpm
Simulation parameters	
Time step, Δt	10^{-5} [s]
Mean particle size, μ	1.7×10^{-3} [m]
Coefficient of variation, CV	0.33
Periodic boundaries, θ	π/32 [rad]
Number of particles, N_p	5000 [#]
Coefficient of friction, μ_f	0.25
Total simulation time, t_{sim}	3 [s]
Powder properties	
Powder	$CaCO_3$
Density, ρ_s	2500 [kg/m^3]
Binder properties	
Binders	Silicon oil and water
Viscosities, μ	1.0, 0.001 [kg/m/s]
Density, ρ_l	997, 1000 [kg/m^3]
Granule properties	
Granule Young's modulus, E	10^7 [Pa]
Granule yield strength, Y_d	10^4 [Pa]
Surface asperity height, h_a	2×10^{-6} [m]

this technique results in some complications to the DEM implementation. Periodic boundaries require that the trajectories for each particle be recalculated once a particle passes through a boundary. Furthermore, contact forces between interacting particles at opposing boundaries must be recalculated to account for the effect of the boundary.

The 5000 particles are distributed in a number-based log-normal distribution with a desired mean size and coefficient of variation displayed in Table 1. Solid and liquid volume fractions are then determined for each particle based on a uniform distribution where the volumes are distributed around a mean shown in Table 1. The air volume is then calculated as the void remaining portion. Since the DEM model is used primarily for calculating collision frequency, no actual coalescence takes place. The total number of particles remains constant. The relevant information for each collision is recorded so that coalescence efficiency could be examined using any coalescence criteria.

A radial boxing scheme was also applied to this simulation to reduce the contact search problem from $O(N(N-1)/2)$ contacts to approximately, $O(N(N-1)/N_{\text{bins}})$. The simulation space was segmented into N_{bins} radial bins, $N_{\text{bins}}=30$ for these simulations. Particles are first sorted into each bin based on radial position. After bin placement, collisions are detected for particles in the same radial bin and the two surrounding radial bins. See Fig. 3 for a representation of the periodic boundary and the boxing scheme.

Simulation speed was also increased using an SGI Altix computer with eight 64-bit Itanium processors. OpenMP was used to automatically parallelize the code. This resulted in a four-fold speed-up.

The algorithm initializes by placing each of the N_{p} granules into the granulator space non-overlapping. The particles are allowed to fall to the base a flat rotor which is not in motion. The particles are allowed to settle for 0.5 s until the rotor begins turning. This creates particle motion. Particles within a neighborhood distance of each other are then allowed to come into contact. Calculations of collision forces occur as normal within a soft-sphere algorithm with one exception: the coefficient of restitution is calculated from the coalescence model as a function of the collision forces. The simulation continues until $t=t_{\text{sim}}$.

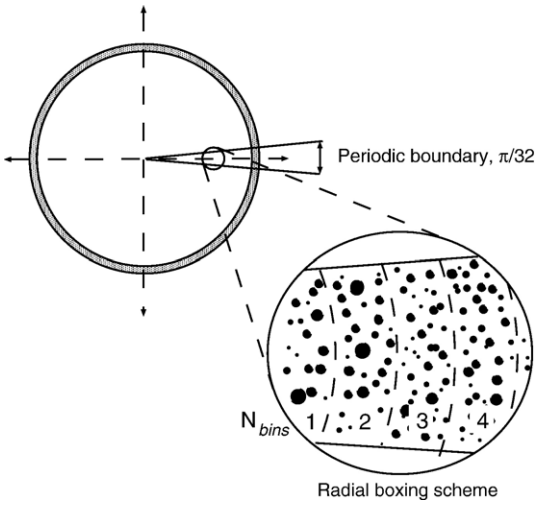

Fig. 3. Boxing scheme applied to a mixer with periodic boundaries.

5. System modeling

5.1. Size-dependent compaction

A multitude of data can be extracted from the DEM simulation. The purpose of this work is to use the data to estimate coalescence kernels and rates of compaction. Iveson et al. [14] proposed a first-order model to describe consolidation behavior by assuming granular porosity approaches a minimum after a large number of collisions:

$$\frac{\mathrm{d}\varepsilon}{\mathrm{d}t} = -k(\varepsilon-\varepsilon_{\min}) \tag{16}$$

In a multidimensional model, the rate of consolidation is an important but poorly understood parameter. Using data from the DEM and coalescence models, impact velocities and the deformability of granules either surface wet or dry can be extracted for consolidation analysis.

Litster and Ennis [15] found that the rate of consolidation was directly related to the granule Stokes deformation number. Litster and Ennis [15] define the rate of compaction, k, empirically as a function of both the rate of collisions, r_{c}, and the Stoke's deformation number, St_{def}:

$$k = r_{\text{c}}\mathrm{e}^{aSt_{\text{def}}} \tag{17}$$

where a is a constant. The rate of collisions, r_{c}, is shown in Fig. 4a as a function of particle size. Due to the log-normal particle size distribution, it is evident that the rate of collisions will be greater among smaller particles.

Fig. 4b shows the size dependence of the Stoke's deformation number. The Stokes deformation number, St_{def}, is a function of collision velocity and granule density. Since the granule density is size-independent, the minimal size dependence of Stoke's deformation number is a result of the collision velocity squared.

From the rate of collisions and the Stoke's deformation number, a size-dependent compaction rate constant can be generated. While rate constants for particle compaction for high-shear granulation is unavailable in literature, rate constants for low-shear processes such as drum are typically $O(10^{-2})$ s^{-1}. A rate constant $O(10^{0})$ s^{-1} for a high-shear granulation process as presented here appears reasonable. Rate constants are presented in Fig. 4c for $a=2e6$ and Fig. 4d for $a=8e6$. These figures show that the rate of compaction is size-dependent due to the rate of collisions rather than the deformation. Therefore, compaction occurs at a faster rate with smaller particles due to the fact that far more small particle will collide with one another.

5.2. Derivation of coalescence kernel

For batch granulation processes, the population balance equation for modeling growth and coalescence is:

$$\frac{\partial n(v,t)}{\partial t} = -\frac{1}{N(t)}\int_{v=0}^{\infty}\beta^{*}(u,v,t)n(u,t)n(v,t)\mathrm{d}v + \frac{1}{2N(t)}\int_{v=0}^{u}\beta^{*}(v,u-v,t)n(v,t)n(u-v,t)\mathrm{d}v \tag{18}$$

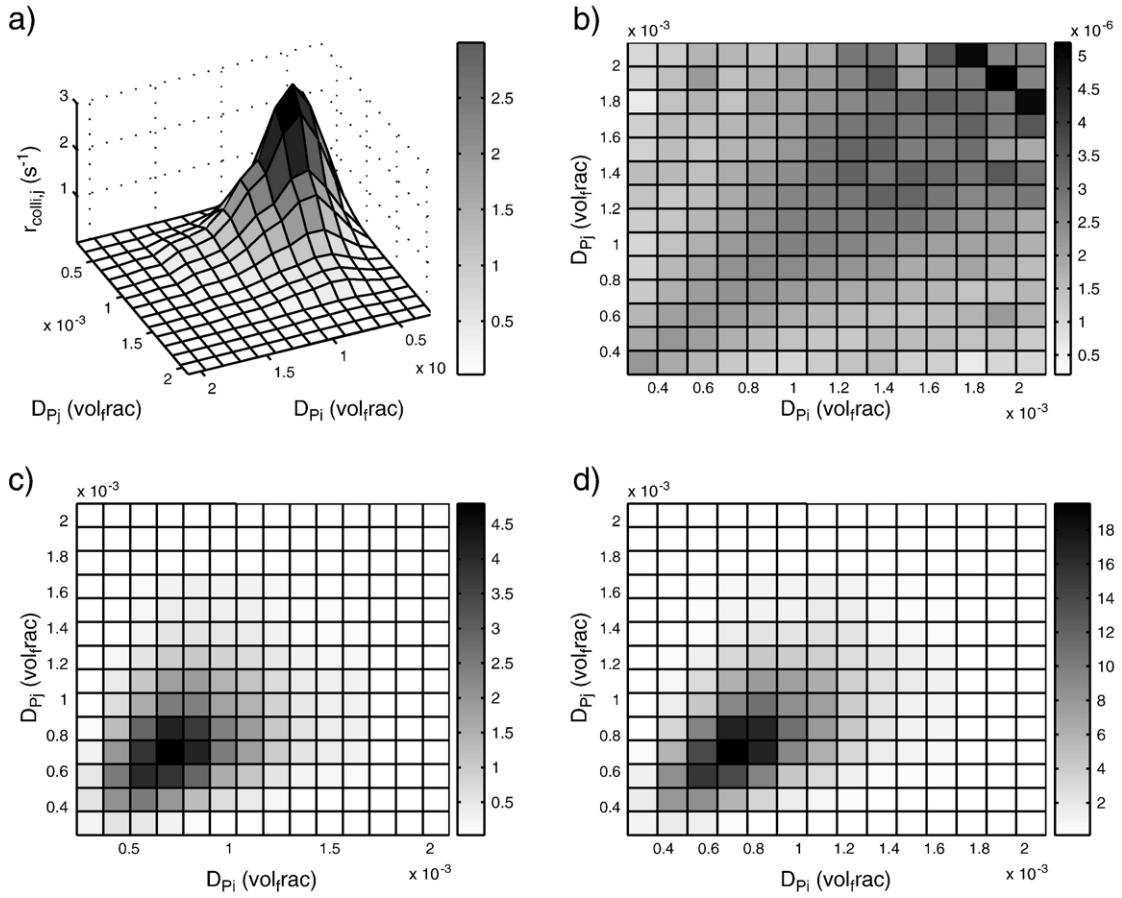

Fig. 4. Several important figures pertaining to consolidation behavior: (a) rate of collisions per particle per second (s^{-1}) as a function of particle size, (b) the Stoke's deformation number, St_{def} (−) as a function of size, (c) a size-dependent consolidation rate constant with $a=2e6$ (s^{-1}), (d) a size-dependent consolidation rate constant with $a=8e6$ (s^{-1}).

where $n(v,t)$ is the number density function, u and v are volumes of coalescing particles, $N(t)$ is the total number of particles at that time, and $\beta(u, v)$ is the coalescence kernel. The coalescence kernel determines how parameter like size and binder content affect coalescence, and is therefore one of the most important factors in modeling granulation.

5.2.1. Multi-scale integration

Development of a coalescence kernel based on analysis of granule scale behavior is a multi-scale problem. While the coalescence kernel is typically written as the product of a size-independent rate constant and a size-dependent term, many of these kernels still require fitting which does not lend itself to a multi-scale model. Tan et al. [16] proposed that the kernel should actually be written as the product of a *collision rate*, $C_{i,j}$, and the *coalescence efficiency*, $\Psi_{i,j}$:

$$\beta_{i,j} = C_{i,j}\Psi_{i,j} \tag{19}$$

Ingram [17] points out that this is "the key equation for developing a multi-scale model". This equation states that there must be some functional form to describe the particle flow and another form to describe coalescence. These models, of course, need to would together to provide a correct estimate at a kernel, but there is no reason that they have to be solved simultaneously. This brings us back to the two models which are available at the micro-scale: the DEM model and the coalescence model. It is the goal of this section to provide a collision rate function, which describes particle flow from the data of the DEM simulation and a coalescence efficiency function from the coalescence model. These two models together will be used to form a coalescence kernel.

The integration scheme is described as follows:

- *Parallel integration:* The coalescence model and the DEM model work in parallel as the coefficient of restitution is calculated using the Coalescence model, yet it is a function of the normal collision velocity supplied by the DEM model. This means that, while both models simulate the granule scale, they are still integrated in parallel.
- *Serial integration:* Serial integration schemes provide a simple relationship used to couple the important data available at the micro-scale to the macro-scale. This provides a simple, efficient, integration scheme at the expense of model flexibility. The data gathered by the DEM/coalescence model will be regressed to form a simple kernel to be used at the unit operation scale.

The collision rate and the coalescence efficiency terms will be determined in two separate sections.

5.2.2. The collision rate function, $C_{i,j}$

Prediction of the rate of collisions has been analyzed by several authors [16–20]. Table 2 presents a list of collision rate functions available in the literature. The collision rate constant can be expressed by the following second-order rate law [16]:

$$r_{ci,j} = C_{i,j} N_i N_j \tag{20}$$

where $r_{ci,j}$ is the rate of collisions between particle sizes i and j, $C_{i,j}$ is the collision rate constant, and N_i is the number of particles size i divided volume of particles in the bed. Given that the simulation time, t_{sim}, and the volume of the powder bed in known, v_{bed}, the collision rate constant can be rewritten as:

$$C_{i,j} = \frac{N_{ci,j}^{PP} v_{bed}}{N_{Pi} N_{Pj} t_{sim}} \tag{21}$$

where $N_{ci,j}^{PP}$ is the number of collisions between particle sizes i and j, and N_{Pi} is the number of particles size i. Each of the proposed forms for collision rate constant found in literature will be compared and the one which provides the best fit with respect to simulation data will be chosen.

- *The size-independent kernel (SIK)* is obviously a very simple kernel first proposed by Kapur and Fuerstenau [4]. The kernel predicts that the rate of coalescence is size-independent and that collisions are completely random in nature. The kernel provides a simple baseline from which a better kernel can be chosen. The kernel can also be a good choice if an analytical solution to the PBE is desired and high model accuracy is not required. The model provides a poor representation of the rate constant surface. If the rate constant were indeed constant, the surface would be identical to the rate of collision surface. A more complex kernel is desired.
- *The equi-partition of kinetic energy kernel (EKE)* is based on the assumption that the kinetic theory of granular flow (KTGF) provides an acceptable description of granular flow in a high-shear mixer. The kinetic theory of granular flow is an extension of the classical kinetic theory of dense gases. It is a statistical mechanical method of describing the mean and fluctuating velocity of particles found in continuous granular media. Processes exemplifying the kinetic theory produce Maxwellian speed distributions with Gaussian distributions for velocity fluctuations in each direction [20]. In the kinetic theory of granular flow, each individual particle velocity, $\bar{v}$, is decomposed into a local mean velocity, $\bar{u}$, and a random fluctuating velocity, $\bar{V}$, described by:

$$\bar{\mathrm{v}} = \bar{\mathrm{u}} + \bar{\mathrm{V}} \tag{22}$$

The kinetic theory assumes that all collisions are binary and instantaneous. In dense flows which are commonly found in high-shear mixers, this assumption may not be valid. Furthermore, a soft-sphere DEM which allows for multiple, long-term collisions may not be the best platform form modeling processes which exhibit behavior in line with the kinetic theory. The KTGF also assumes particles are spherical, smooth and elastic. Granules produced experimentally may be neither of these. In fact, the most obvious drawback is the fact that several sources report coefficients of restitution between 0.01 and 0.4 which is far from elastic [14,21].

- *The equi-partition of translational momentum kernel (ETM)* is derived in much the same manner as the EKE kernel except that instead of assuming that there is equally distributed kinetic energy, an equal distribution of random fluctuating granule impulses is assumed. Therefore, the random component of the translational momentum remains constant. This couples with the assumption provided in kinetic theory that collisions are elastic in nature and all energy is manifested in translational kinetic energy. The authors felt that assumption was implausible and thus decided each granule is subject to the same random fluctuating impulses so that the random fluctuating velocity. The derivation of this kernel relies heavily on numerous assumptions which may or may not be physically relevant.
- *The perikinetic or Brownian motion kernel (PK)* was first presented by Smoluchowski in 1917 [22] who proposed two separate collision mechanisms: perikinetic and orthokinetic. Perikinetic motion is induced by random, diffusive motion of particles. While assuming collisions are randomin nature, similarly as to what is proposed by the kinetic theory, perikinetic motion typically occurs almost motionless media between very small flocculants. Neither of these assumptions appear to be adequate when describing motion in a high-shear mixer.
- *The induced shear kernel (ISK)* also known as orthokinetic motion was also presented by Smoluchowski in 1917 [22]. Smoluchowski analyzed the rate of collisions among spherical particles in a laminar shear flow, $(u_x, u_y, u_z)=(\Gamma y, 0, 0)$ with a constant gradient of $\partial u_x/\partial y=\Gamma$. The rate of collisions between particle sizes i and j can them be calculated by:

$$r_{\mathrm{coll}\ i,j} = N_i N_j \int_{w_r<0} -w_r \mathrm{d}A \tag{23}$$

where w_r is the radial component of the relative velocity between particles i and j, and A is the collision area surface with

Table 2
Collision rate functions found in literature

Collision rate function, $C_{i,j}$	Name	Reference
$C_{i,j} = k$	Size-independent kernel (SIK)	[4,28]
$C_{i,j} = (l_i + l_j)^2 \sqrt{\frac{1}{l_i^3} + \frac{1}{l_j^3}}$	Equi-partition of kinetic energy kernel (EKE)	[16,20]
$C_{i,j} = (l_i + l_j)^2 \sqrt{\frac{1}{l_i^6} + \frac{1}{l_j^6}}$	Equi-partition of translational momentum kernel (ETM)	[19]
$C_{i,j} = \frac{(l_i + l_j)}{l_i l_j}$	Perikinetic or Brownian motion kernel (PK)	[22]
$C_{i,j} = (l_i + l_j)^3$	Orthokinetic or induced shear kernel (ISK)	[22]

radius R_{ij}. In spherical coordinates (R, θ, ϕ), the relative velocity can be rewritten as, $w_r = \Gamma y \cos\theta$. Defining $dA = R_{i,j}^2 \sin\theta d\theta d\phi$, the rate of collisions can be written as:

$$r_{\text{coll } i,j} = N_i N_j \frac{4}{3} \Gamma R_{i,j}^3 \tag{24}$$

Several important observations should be pointed out. First, the ISK kernel assumes that particles collide as a consequence of a laminar shearing motion. While there is definitely shearing motion found in the granulator, it may not best be described as a simple laminar flow. If turbulent flow is dominant in the mixer, one may assume that collisions result due to random motion, similar as to that described by the EKE kernel.

Comparing each of these established collision rate functions, one can tell each provides a mechanistically based form at the expense of multiple assumptions. Fig. 5 shows how the collision rate coefficient extracted from DEM data compares to the functional forms of the collision rate function previously presented. As shown in this figure, the collision rate extracted from the data presents a very discontinuous surface which cannot be approximated by a size-independent kernel. The shear kernel shows that that large–large particle collisions are preferential and most common, which is also shown from the extracted DEM data. Both the EKE and the ETM kernels favor large–small particle collisions, which seems to not be the most accurate model. This is possibly due to the low coefficient of restitution and non-ideal behavior found in the mixer. This also

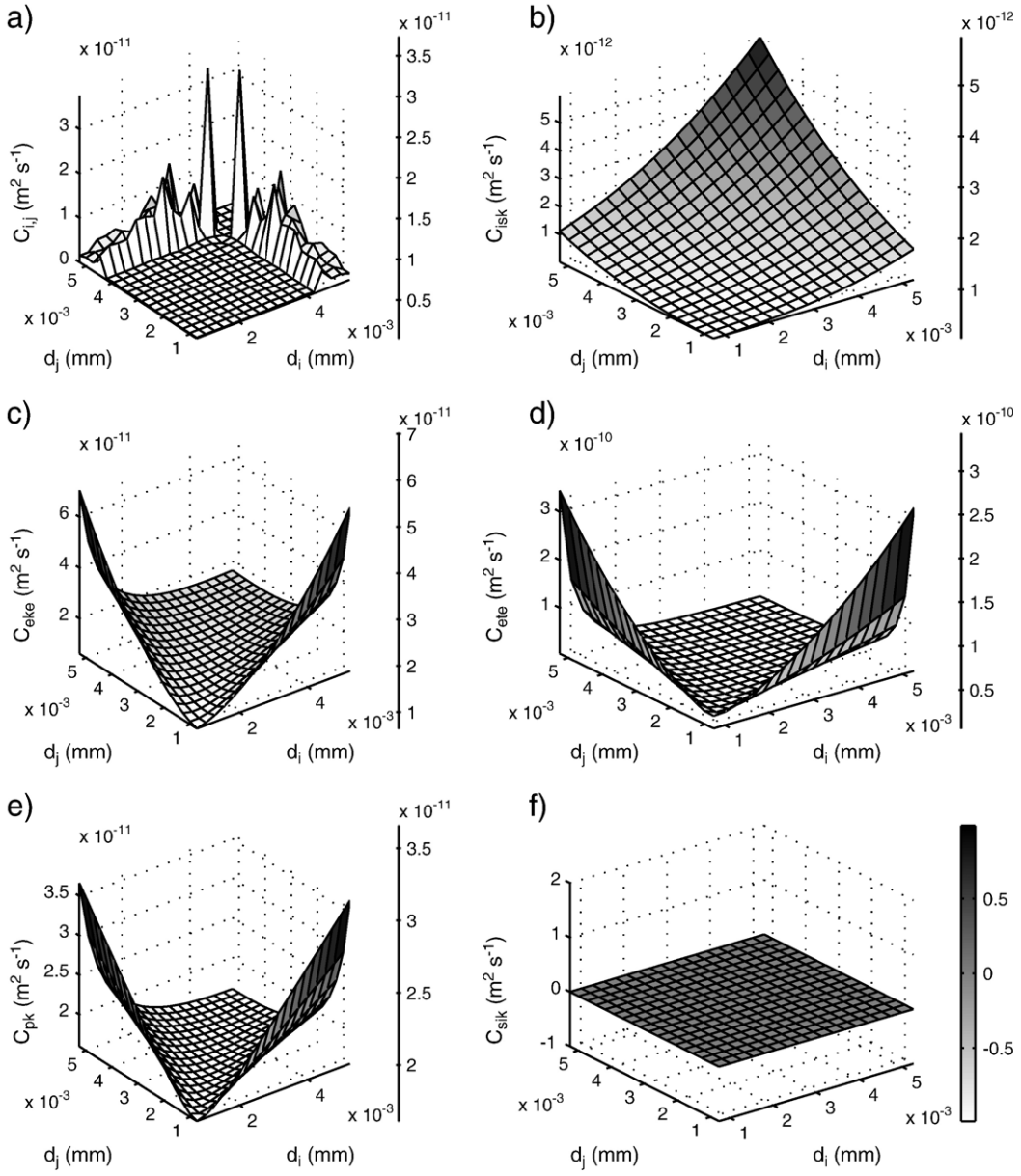

Fig. 5. A comparison of collision rate functions found in literature to DEM/coalescence simulation results: (a) simulation results, (b) ISK kernel, (c) EKE kernel, (d) ETM kernel, (e) PK kernel and (f) SIK kernel.

Table 3
Coalescence efficiency results for simulations comparing two different binders

	a_0	a_1	a_2	a_3	a_4	Probability
Water						
Type I	−0.001	0.10	0.001	0.001	−0.002	4.8×10^{-3}%
Type II	−1.76	93.47	1.85	1.43	0.02	4.64%
Overall	−1.76	93.47	1.85	1.43	0.02	4.64%
Si oil						
Type I	−1.11	54.62	1.18	0.91	−0.05	2.77%
Type II	−0.79	26.96	0.85	0.58	0.06	2.30%
Overall	−1.90	81.58	2.03	1.49	0.01	5.07%

shows that collisions in high-shear mixers are commonly a result of the shear forces as opposed to the random fluctuations and that the shear kernel may be a preferential model for particle collision rates. It should be noted that other parameters in addition to particle size (pore saturation, porosity, particle velocity) were also analyzed to determine their effect on collision rate and it was determined that only particle size significantly influenced collision rate.

5.2.3. The coalescence efficiency function, $\Psi_{i,j}$

Particle size is not the only factor when analyzing particle coalescence. An accurate coalescence efficiency function needs to incorporate several other factors into the coalescence kernel which affect growth dynamics. Iveson [23] presents a survey of granulation literature which shows that granule porosity, pore saturation and particle size independently influence granule growth behavior and final product properties. Furthermore, Iveson [24] concludes that one-dimensional models are unable to account for all of these effects, requiring the development of a multi-dimensional model. Therefore, the proposed coalescence efficiency function will be multidimensional in nature and will include the following internal parameters in addition to size:

- *Pore saturation:* It is well understood that granule compaction plays a role in coalescence behavior [1,14]. Newly nucleated particles are loosely held together by narrow liquid bridges. This state of pore saturation is called the pendular state. As compaction continues, granules strengthen and liquid is slowly forced through the pores until a critical pore saturation is reached and a binder layer is formed [14]. Rapid growth typically follows the formation of a binder layer. For this reason, pore saturation will be used in this model.
- *Porosity:* Porosity directly determines deformability and strength of a granule. Soft, less porous particles are more likely to deform, and therefore may be more likely to coalesce in highly deformable granulation processes. Furthermore, Annapragada and Neilly [25] state that porosity should be incorporated into a realistic agglomeration model. As particles compact, they become denser and stronger. Annapragada and Neilly [25] state that, as granules increase in density and strengthen, breakage rates decrease and coalescence effects dominate. Several existing coalescence models depend on the porosity of granules (Thornton and Ning [26] and Liu et al. [13]). This simulation intends to show how porosity effects coalescence for the agglomeration process described.
- *Particle velocity:* Particle impact velocity, u, has also proven to play a role in coalescence behavior. As the impeller speed increases, the rate of compaction increases and deformability plays a greater role. Furthermore, if one assumes that particle collision speed is proportional to the impeller speed, then the kernel developed is then more suitable for control studies as impeller speed is a simple manipulated tool for the process.

A multidimensional population balance is proposed which uses solid volume of particles, liquid volume of particles, air volume of particles and impeller speed as internal coordinates. By accounting for solid, s, liquid, l, and air volume, a, one can easily calculate particle diameter, $D=2(3(s+l+a)/(4\pi))^{1/3}$, pore saturation, $S=l/(s+l)$, and porosity, $\varepsilon=(l+a)/(s+l+a)$.

From results gathered from DEM/coalescence model simulations, an estimation for $\Psi_{i,j}$ as a function of particle size, pore saturation and porosity can be made, $\Psi_{i,j}=f(D, S, \varepsilon, u)$. During a simulation, the solid, liquid and air volumes as well as the impeller speed for each collision event are saved in a matrix, A. Following each collision, criteria for type I and type II coalescence are calculated. A resulting vector, b, stores a 1 for successful collisions and 0 for unsuccessful collisions. Using the DEM data, a simple regression can be used to map the collision

Table 4
Categorized regression coefficients for a silicon oil binder simulation

Model	a_0	a_{D_i}	a_{S_i}	a_{ε_i}	a_{D_j}	a_{S_j}	a_{ε_j}	a_u	Probability	$D_i>D_j$	$S_i>S_j$	$\varepsilon_i>\varepsilon_j$
Water												
1	−1.76	19.08	1.05	−1.62	28.56	0.06	3.89	0.02	11.22%	1	1	1
2	−2.04	97.90	2.43	2.09	−4.90	−0.45	−0.93	0.03	38.87%	1	1	0
3	−1.48	−4.21	−0.03	−0.93	172.70	1.46	1.22	0.01	39.10%	1	0	1
4	−0.90	−11.09	0.13	1.92	30.51	0.32	−0.58	−0.02	10.80%	1	0	0
Si oil												
5	−1.18	−259.40	1.99	0.18	15.77	0.15	−0.01	0.01	26.83%	1	1	1
6	−0.87	−93.79	1.22	0.53	−135.13	0.48	−0.15	0.06	33.70%	1	1	0
7	−0.93	−307.11	0.78	−0.35	110.06	0.99	0.81	0.01	7.07%	1	0	1
8	−1.59	−73.19	0.13	0.11	−39.99	2.14	0.26	0.03	32.40%	1	0	0

information, s_i, l_i, a_i, s_j , l_j , a_j and u to a coalescence efficiency, $\Psi_{i,j}$.

The equation for the linear regression is expressed as:

$$\Psi_{i,j} = a_0 + a_1\overline{\mathrm{D}}_{i,j} + a_2\overline{\mathrm{S}}_{i,j} + a_3\overline{\varepsilon}_{i,j} + a_4 u \tag{25}$$

A vector of coefficients, $x=[a_0\ a_1\ \ldots\ a_4]^T$, is solved using the pseudo-inverse in the following manner:

$$Ax = b \tag{26}$$

$$x = (A^T A)^{-1} A^T b \tag{27}$$

where A is an $N\times 5$ matrix describing each parameter for N total collisions. A uniform distribution of solid and liquid volume fractions allow for a wide distribution of the pore saturations and porosities for particles in the simulation. This is done to capture a wide range of possible interactions.

6. Results

Two simulations were performed, each with identical conditions as presented in Table 1 with the exception of binder viscosities. Table 3 compares regression results from both simulations. Analysis of the regressed data shows that increasing particle size, pore saturation and porosity each increase the coalescence efficiency. Furthermore, while the mode of coalescence was greatly influenced by the viscosity of the binder, the overall efficiency was not. It should be noted that sensitivity to process parameters which may not be very well defined may play a role in this.

Interactions between particles i and j form a symmetric A matrix. Modeling this matrix as a plane, as presented previously, presents many issues which are alleviated when order is applied to the system. Since this is a multidimensional problem, adding order to the problem produce distinctly different kernels depending on the regime. For each collision, the colliding particles will be put into one of four possible categories according to their size, pore saturation and porosity. This provides four distinct kernels. To begin sorting, particle i will always be the larger particle by total volume. The method sorts then based on pore saturation and porosity. The four categories and the final results of this regression are presented in Table 4. Note that, while there are more coefficients, the general trends can still be identified. Smaller, porous, saturated particles generally have a greater chance of coalescence. Also note that the coefficients tend to be higher with the silicon binder leading to the conclusion that more viscous binders have a higher rate of coalescence.

The collision rate function which best fits the DEM data provides was determined to be the induced shear kernel. A multidimensional coalescence efficiency function was then regressed from simulation data in multiple forms. The coalescence model used only accounts for binary, head-on collisions. An artificially high coalescence efficiency may possibly be reported by assuming that the tangential component of the collision is in effect negligible. Analysis of the DEM/coalescence model data shows that the tangential component appears to be important, a fact also recognized by Ingram [17] when analyzing drum granulation behavior. This is seen in the mean value of the ratio of the tangential to normal component of the collision velocity, $|u_t/u_n|=1.96$. This means that in many cases, the tangential component cannot be ignored. One solution is to use a critical value of this ratio which states that the normal component of the relative velocity must be several times larger than the tangential component for coalescence to occur. For instance, if $|u_t/u_n|^*=1/20$ is the critical number, only 2.93% of possible collisions can actually agglomerate in the current work. This factor can help account for the discrepancy between these and other published efficiency values.

Together, the final multi-scale coalescence kernel can be presented as:

$$\beta_{i,j} = \zeta\frac{4}{3}\Gamma\left(d_i + d_j\right)^3\left(a_0 + a_1\overline{D}_{i,j} + a_2\overline{S}_{i,j} + a_3\overline{\varepsilon}_{i,j} + a_4 u\right) \tag{28}$$

where ζ is the fraction of collisions which have a ratio of the tangential to normal collision velocities which are greater than a critical number. This kernel ultimately separates the efficiency $\Psi_{i,j}$ and the frequency $C_{i,j}$ as:

$$\Psi_{i,j} = \zeta(a_0 + a_1\overline{D}_{i,j} + a_2\overline{S}_{i,j} + a_3\overline{\varepsilon}_{i,j} + a_4 u)$$

$$C_{i,j} = \frac{4}{3}\Gamma\left(d_i + d_j\right)^3$$

For this work, $\zeta=1.0$, indicating the tangential component was neglected.

7. Conclusions

A DEM model of a high-shear mixer was used with a physically relevant model of coalescence to model coalescence events at the micro-scale. The DEM approach used a novel boxing scheme and periodic boundaries to reduce the computation time, but maintain velocity flow fields which are observed experimentally. Using the data produced from the DEM simulation, a size-dependent compaction rate and a multidimensional coalescence kernel were calculated for future application in a population balance model. The kernel was solved by decoupling the effect of collision rates and collision efficiency. The induced shear collision rate function provided the best representation of simulation data since it predicted large–large particle collision are preferential (as seen in simulation data). A multidimensional coalescence efficiency was calculated using two different regression techniques from DEM simulation data. This unique method of calculating a multidimensional coalescence kernel will soon be used in collaboration with a Monte-Carlo solution technique of a population balance model, therefore bridging the micro-scale to the meso-scale.

Notation

a_i	Regressed collision rate constants
$C_{i,j}$	Collision rate function, m^3/s
D	Particle diameter, m
e	Coefficient of restitution
E	Particle Young's modulus, N/m^2

$\overrightarrow{F_c}$	Particle collision forces, N
$\overrightarrow{F_n}$	Normal contact forces, N
$\overrightarrow{F_t}$	Tangential contact forces, N
$\overrightarrow{F_w}$	Wall collision forces, N
$\overrightarrow{g}$	Gravitational acceleration vector, m/s^2
h_0	Binder layer thickness, m
h_a	Surface asperity thickness, m
k	Rate of compaction, s^{-1}
k_n	Normal spring constant, N/m
k_t	Tangential spring constant, N/m
l_i	Diameter of particle i, m
m	Particle mass, kg
N_i	Number density of particles size i, m^{-3}
N_{Pi}	Total number of particles size i
$N^{PP}_{\text{coll } i,j}$	Total number of particles which have collided in the classes i and j
$\overrightarrow{r}$	Particle position vector, m
$\overrightarrow{r_0}$	Particle position vector, m
s	Particle pore saturation
s^*	Critical pore saturation
St_v	Viscous Stokes' number
St_{def}	Stokes' deformation number
Δt	Time step, s
t_d	Contact duration, s
v_{bed}	Total volume of the particle bed (void space included), m^3
$\overrightarrow{v}$	Particle velocity vector, m/s
$\overrightarrow{v_n}$	Normal collision velocity vector, m/s
$\overrightarrow{v_t}$	Tangential collision velocity vector, m/s
$\overrightarrow{v_0}$	Particle velocity vector, m/s
Y_d	Granule yield strength, N/m^2

Greek letters

β	One-dimensional coalescence kernel
δ''	Permanent particle deformation, m
ε	Particle porosity
ζ	Tangential rejection factor
η	Damping coefficient, m/s
μ	Binder viscosity, kg/m/s
μ_f	Coefficient of friction
ξ	Tangential overlap, m
$\Psi_{i,j}$	Coalescence efficiency
Ω	Multidimensional coalescence kernel

Acknowledgments

The author would like to acknowledge valuable discussions with Dr. Gordon Ingram and Dr. Lian Liu. Additionally, the authors are grateful for the comments and suggestions of the anonymous reviewers.

References

[1] B.J. Ennis, Agglomeration and size enlargement session summary paper, Powder Technology 88 (1996) 203–225.
[2] I.T. Cameron, Modern process modelling: multiscale and goal-directed, Proceedings of the 14th International Drying Symposium, vol. A, 2004, pp. 3–17.
[3] P.C. Kapur, D.W. Fuerstenau, Kinetics of green pelletisation, Trans. AIME 229 (1963) 348–355.
[4] P.C. Kapur, D.W. Fuerstenau, Coalescence model for granulation, Industrial and Engineering Chemistry, Process Design Devices 8 (1969) 56–62.
[5] P.C. Kapur, Kinetics of granulation by non-random coalescence mechanism, Chemical Engineering Science 27 (1972) 1863–1869.
[6] K. Sastry, D. Fuerstenau, Size distribution of agglomerates in coalescing disperse phase systems, Industrial and Engineering Chemistry, Fundamentals 9 (1970) 145–149.
[7] K.V.S. Sastry, D.W. Fuerstenau, Mechanisms of agglomerate growth in green pelletization, Powder Technology 7 (1973) 97–105.
[8] A.A. Adetayo, B.J. Ennis, A new approach to modeling granulation processes for simulation and control purposes, Powder Technology 108 (2000) 202–209.
[9] L.X. Liu, J.D. Litster, Population balance modeling of granulation with a physically based coalescence kernel, Chemical Engineering Science 57 (2002) 2183–2191.
[10] P.A. Cundall, O.D.L. Strack, A distinct element model for granular assemblies, Geotechnique 29 (1979) 47–65.
[11] Y. Muguruma, T. Tanaka, Y. Tsuji, Numerical simulation of particulate flow with liquid bridge between particles (simulation of centrifugal tumbling granulator), Powder Technology 109 (2000) 49–57.
[12] J. Schafer, S. Dippel, D.E. Wolf, Force schemes in simulations of granular material, Journal of Physics I (France) 6 (1996) 5–20.
[13] L.X. Liu, J.D. Litster, S.M. Iveson, B.J. Ennis, Coalescence of deformable granules in wet granulation processes, AIChE Journal 46 (3) (March 2000) 529–539.
[14] S. Iveson, J. Litster, B. Ennis, Fundamental studies of granule consolidation: Part 1. Effects of binder content and binder viscosity, Powder Technology 88 (1996) 15–20.
[15] J. Litster, B.J. Ennis, The Science and Engineering of Granulation Processes, Volume 1, Kluwer Academic, 2004.
[16] H. Tan, M. Goldschmidt, R. Boerefijn, M. Hounslow, A. Salman, J. Kuipers, Building population balances for fluidized bed granulation: lessons from kinetic theory of granular flow, Powder Technology 142 (30) (2004) 103–109.
[17] G.D., Ingram. PhD thesis, University of Queensland, St. Lucia, Queensland, AU, 2006.
[18] A. Darelius, A. Rasmuson, I.N. Bjorn, S. Folestad, High shear wet granulation modelling—a mechanistic approach using population balances, Powder Technology 160 (2005) 209–218.
[19] M.J. Hounslow, The population balance as a tool for understanding particle rate processes, Kona, 1998, pp. 179–193.
[20] M. Goldshmidt. Hydrodynamic modelling of fluidized bed granulation. PhD thesis, Twente University, 2001.
[21] C. Mangwandi, J. Fu, G. Reynolds, M. Adams, M. Hounslow, A. Salman. Impact behavior of different types of granules. In 8th International Symposium on Agglomeration, pages 11–21, 447 Sri Ayudhaya rd, Bangkok, Thailand, 2005. The Industrial Pharmacists Group.
[22] M. Smoluchowski, Versuch einer matematischen theorie der koagulationskinetic kolloider lösungen, Zeitschrift für Physikalische Chemie (1917) 129–168.
[23] S.M. Iveson, Limitations of one-dimensional population balance models of wet granulation processes, Powder Technology 124 (2002) 219–229.
[24] S.M. Iveson, J.A. Beathe, N.W. Page, The dynamic strength of partially saturated powder compacts: the effect of liquid properties, Powder Technology 127 (2002) 149–161.
[25] A. Annapragada, J. Neilly, On the modelling of granulation processes: a short note, Powder Technology 89 (1996) 83–84.
[26] C. Thornton, Z. Ning, A theoretical model for the stick/bounce behavior of adhesive, elastic–plastic spheres, Powder Technology 99 (1998) 154–162.
[27] T. Tsuji, T. Kawaguchi, T. Tanaka, Discrete particle simulation of two-dimensional fluidized bed, Powder Technology 77 (1993) 79–87.
[28] M.J. Hounslow, J.M.K. Pearson, T. Instone, Tracer studies of high-shear granulation: II. Population balance modeling, AIChE 47 (2001) 1984–1999.